Journal of Virology

Virology | Full-Length Text

Secreted phospholipase PLA2G2E contributes to regulation of T cell immune response against influenza virus infection

Hemeng Bu,[1,2] Shengnan Zhang,[1] Pingchao Li,[1] Zijian Liu,[1,2] Yichu Liu,[1] Zhixia Li,[1] Xinglong Liu,[1,2] Zhi Wang,[1] Liqiang Feng,[1] Ling Chen,[1] Linbing Qu[1]

AUTHOR AFFILIATIONS See affiliation list on p. 17.

ABSTRACT The involvement of secreted phospholipase A2s in respiratory diseases, such as asthma and respiratory viral infections, is well-established. However, the specific role of secreted phospholipase A2 group IIE (PLA2G2E) during influenza virus infection remains unexplored. Here, we investigated the role of PLA2G2E during H1N1 influenza virus infection using a targeted mouse model lacking *Pla2g2e* gene (*Pla2g2e*$^{-/-}$). Our findings demonstrated that *Pla2g2e*$^{-/-}$ mice had significantly lower survival rates and higher viral loads in lungs compared to wild-type mice following influenza virus infection. While *Pla2g2e*$^{-/-}$ mice displayed comparable innate and humoral immune responses to influenza virus challenge, the animals showed impaired influenza-specific cellular immunity and reduced T cell-mediated cytotoxicity. This indicates that PLA2G2E is involved in regulating specific T cell responses during influenza virus infection. Furthermore, transgenic mice expressing the human *PLA2G2E* gene exhibited resistance to influenza virus infection along with enhanced influenza-specific cellular immunity and T cell-mediated cytotoxicity. *Pla2g2e* deficiency resulted in perturbation of lipid mediators in the lung and T cells, potentially contributing to its impact on the anti-influenza immune response. Taken together, these findings suggest that targeting *PLA2G2E* could hold potential as a therapeutic strategy for managing influenza virus infections.

IMPORTANCE The influenza virus is a highly transmissible respiratory pathogen that continues to pose a significant public health concern. It effectively evades humoral immune protection conferred by vaccines and natural infection due to its continuous viral evolution through the genetic processes of antigenic drift and shift. Recognition of conserved non-mutable viral epitopes by T cells may provide broad immunity against influenza virus. In this study, we have demonstrated that phospholipase A2 group IIE (PLA2G2E) plays a crucial role in protecting against influenza virus infection through the regulation of T cell responses, while not affecting innate and humoral immune responses. Targeting PLA2G2E could therefore represent a potential therapeutic strategy for managing influenza virus infection.

KEYWORDS influenza virus, PLA2G2E, survival, T cell-mediated cytotoxicity

Influenza virus is transmitted through the respiratory tract and typically results in a spectrum of diseases, ranging from mild respiratory illness to severe pneumonia in humans. Annually, influenza virus infection accounts for approximately 10% of all infectious diseases worldwide and is responsible for an estimated 500,000 fatalities (1). Influenza viruses can be classified into influenza A, B, and C virus according to the antigenicity of nucleocapsid and matrix proteins, of which influenza A virus is capable of infecting and is the most pathogenic. Vaccination is currently the most effective strategy to control influenza epidemics, but the effectiveness of vaccination has been poor in certain years (2). Current influenza vaccines primarily elicit humoral immune responses

Editor Paul G. Thomas, St. Jude Children's Research Hospital, Memphis, Tennessee, USA

Address correspondence to Ling Chen, chen_ling@gibh.ac.cn, or Linbing Qu, qu_linbing@gibh.ac.cn.

Hemeng Bu and Shengnan Zhang contributed equally to this article. Author order was determined alphabetically and in order of increasing seniority.

Pingchao Li, Ling Chen, and Linbing Qu contributed equally to this article. Author order was determined by increasing contributions to the article.

The authors declare no conflict of interest.

See the funding table on p. 17.

Received 7 February 2024
Accepted 24 March 2024
Published 9 April 2024

targeting the globular head region of hemagglutinin (HA) protein from vaccine strains (3). The occurrence of antigenic drift and shift in viral surface proteins, HA and neuraminidase (NA), enables evasion of host immune system, leading to seasonal influenza epidemics (4).

In comparison to humoral immunity, cellular immunity exhibits greater cross-reactivity and efficacy in eliminating all subtypes of influenza virus, because T cells recognize internal and highly conserved regions of influenza virus that are less susceptible to mutation (5). Previous studies have emphasized the significance of T cell-mediated immunity in protection against influenza virus infection. Transfer of antigen-specific $CD4^+$ and $CD8^+$ T cells into naive recipient mice confers protection against heterologous strains of influenza virus (6–8). Furthermore, the depletion of memory T cells in mice previously recovered from influenza virus infection heightens their susceptibility to subsequent infections (9, 10). Lipid mediator prostaglandin E2 (PGE2) suppresses T cell recruitment and delays the initiation of influenza A virus antigen-specific T cell response in lungs of influenza virus-infected mice (11). Oral administration of eicosapentaenoic acid and docosahexaenoic acid (DHA) significantly attenuates the pulmonary $CD8^+$ T cell response in mice infected with PR8 virus (12).

The secreted phospholipase A2 (sPLA2) family selectively catalyzes the hydrolysis of ester bonds at the sn-2 site of phospholipid diastereomers, resulting in the production of lysophospholipids and free fatty acids (13). sPLA2 plays an important role in the production of lipid mediators, maintenance of membrane homeostasis, exertion of antimicrobial activity, and regulation of lipid metabolism across various tissues (14). Previous study has demonstrated that phospholipase A2 group IID (PLA2G2D), a member of the sPLA2 family, impedes the migration of respiratory dendritic cells from the respiratory tract to the draining lymph nodes during influenza virus, severe-acute-respiratory-syndrome-related coronavirus (SARS-CoV), and SARS-CoV-2 infection (15, 16). The expression of another sPLA2, PLA2G2A, is significantly upregulated and exhibits elevated enzyme activity during SARS-CoV-2 virus infection, thereby being implicated in the pathobiology underlying Coronavirus disease 2019 (COVID-19) mortality (17).

PLA2G2E, a member of the group II subfamily within the sPLA2 family, exhibits low levels of expression in tissues under physiological conditions and is primarily localized to glutamate-rich tissues. The marked upregulation of PLA2G2E expression in alveolar macrophages in response to lipopolysaccharide (LPS) stimulation underscores its pivotal role in immune activation (18–20). We reanalyzed the publicly available transcriptomic data (21–23) and observed a significant upregulation of PLA2G2E expression in both lung epithelial cells and alveolar macrophages in C57BL/6 mice following H1N1 A/WSN/1933 virus infection compared to uninfected mice. However, the roles of PLA2G2E in viral infection remain unclear. Therefore, in this study, we used influenza as a model of viral infection and assessed the antiviral and immunomodulatory effects of PLA2G2E during influenza virus infection by using *Pla2g2e*$^{-/-}$ mice and human *PLA2G2E* gene transgenic mice.

RESULTS

Pla2g2e-deficient mice exhibit heightened susceptibility to influenza virus infection

We initially confirmed that H1N1 A/Puerto Rico/8/1934 (PR8) infection significantly upregulated the expression of PLA2G2E in two human lung cancer cell lines, A549 and NCI-H1299, as well as in wild-type C57BL/6N mice at 8 weeks and 6 months of age (Fig. S1A through D). We further found that PR8 infection induced an increase in PLA2G2E expression mainly in lung epithelial cells, but not in alveolar macrophages and endothelial cells (Fig. S1E). This is not completely consistent with the WSN infection model reported in the literature (21–23). Additionally, we observed that the expression of PLA2G2E remained unaltered with advancing age (Fig. S1F).

To investigate the role of PLA2G2E in the pathogenesis of influenza virus infection, we employed a previously generated C57BL/6 mouse model with systemic *Pla2g2e* gene

knockout (24). Eight-week-old wild-type (WT) and *Pla2g2e*$^{-/-}$ mice were inoculated with 1,500 plaque-forming units (PFU) of PR8 virus, and the body weight and survival rate of the animals were monitored for 14 days post-infection (p.i.). *Pla2g2e*$^{-/-}$ mice displayed a significantly delayed recovery of body weight (Fig. 1A) and had higher mortality rates (Fig. 1B) compared to those of WT mice. The viral titers in lung tissues of WT and *Pla2g2e*$^{-/-}$ mice were assessed using quantitative PCR and plaque assays on days 3, 7, and 10 p.i. On days 7 and 10 p.i., the lung viral RNA loads in *Pla2g2e*$^{-/-}$ mice were significantly higher than that in WT mice, while no significant difference was observed on day 3 p.i. (Fig. 1C). Additionally, *Pla2g2e*$^{-/-}$ mice exhibited a comparable infectious viral titer to WT mice on day 3 p.i. (Fig. 1D), while displaying a higher infectious viral titer on day 7 p.i. (Fig. 1E). By day 10 p.i., infectious viruses were undetectable in both WT and *Pla2g2e*$^{-/-}$ mice (Fig. 1F). These findings suggest a less efficient clearance of influenza virus in *Pla2g2e*$^{-/-}$ mice compared to their WT counterparts. However, there were no significant differences observed in the pulmonary pathological changes between WT

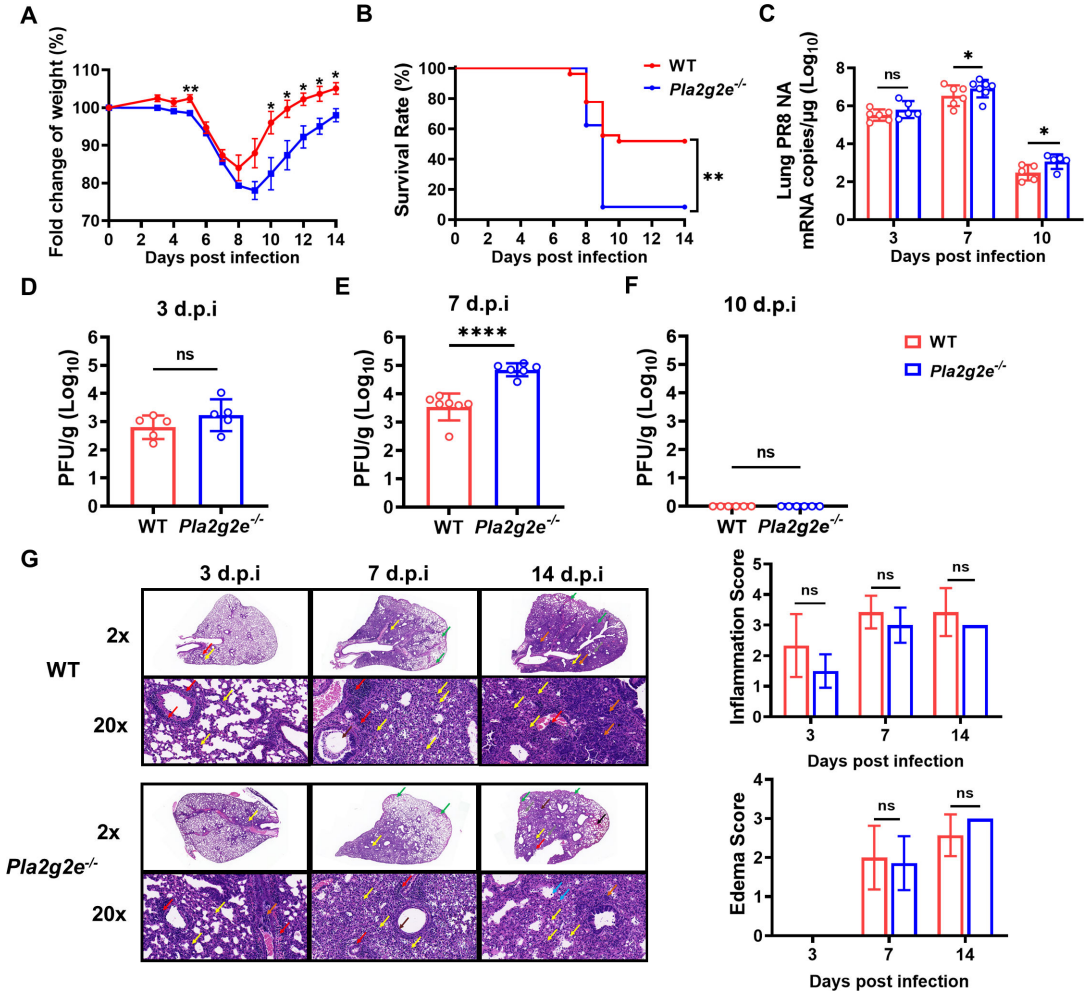

FIG 1 *Pla2g2e*-deficient mice exhibit heightened susceptibility to influenza virus infection. (A and B) WT (n = 27) and *Pla2g2e*$^{-/-}$ (n = 24) mice were intranasally infected with 1,500 PFU of PR8 virus. Body weight (A) and survival (B) of PR8-infected mice were monitored daily for 14 days. (C–F) WT and *Pla2g2e*$^{-/-}$ mice were intranasally infected with 1,500 PFU of PR8 virus, and lung tissues were collected on days 3, 7, and 10 p.i., with a sample size of n = 5–7 for each time point. (C) Viral loads in the lung tissues of PR8-infected mice were evaluated using quantitative RT-PCR. (D–F) Viral titers in the lung tissues collected at different time points were assessed by plaque formation assay. (G) H&E staining of lung tissues from PR8-infected WT and *Pla2g2e*$^{-/-}$ mice on days 3, 7, and 14 p.i. Yellow arrows indicate granulocytic infiltrates; red arrows indicate small focal infiltrates of lymphocytes; orange arrows indicate endothelial cell hyperplasia; blue arrows indicate macrophages; green arrows indicate eosinophilic histological fluid; gray arrows indicate alveolar dilatation. The criteria for inflammation scores and pulmonary edema scores were described in Materials and Methods section. Mean ± SD; two independent experiments, 4–7 mice per group. *, $P < 0.05$; **, $P < 0.01$; ***, $P < 0.001$; ****, $P < 0.0001$; ns, $P > 0.05$. Bar: (2×) 500 µm; (20×) 50 µm.

and *Pla2g2e*$^{-/-}$ mice. Hematoxylin and eosin (H&E) staining revealed comparable wall thickening and inflammatory cell infiltration in both groups on days 7 and 14 p.i., accompanied by occasional hemorrhage and pulmonary edema (Fig. 1G). The expression levels of chemokines (CCL2, CCL3, CCL5, CXCL2, CXCL5, and CXCL10) and proinflammatory cytokines (IL-1β, IL-6, and IL-8) were upregulated in lung tissues of WT and *Pla2g2e*$^{-/-}$ mice and exhibited comparable expression levels between two groups (Fig. S2). These findings imply that PLA2G2E confers protection against mortality associated with influenza A virus infection in mice.

Pla2g2e-deficient mice have comparable innate and humoral immune responses to influenza virus challenge

Innate immunity serves as the first line of antiviral defense and is indispensable for mounting an effective antiviral immune response. interferon (IFN) responses to RNA viruses, such as influenza virus, are initiated by viral [single-strand RNA (ssRNA) and double-strand RNA (dsRNA) binding to pattern recognition receptors. The expression levels of retinoic acid-inducible gene-I (RIG-I)-like receptors [RIG-I and melanoma differentiation-associated protein 5 (MDA5)] and Toll-like receptors (TLR3 and TLR4), as well as their downstream signaling proteins (MAVS and IRF1), were upregulated in lung tissues of *Pla2g2e*$^{-/-}$ mice, consistent with the expression patterns of WT mice (Fig. 2A). In response to PR8 challenge, WT and *Pla2g2e*$^{-/-}$ mice had comparable transcriptional levels of interferons (Fig. 2B) and interferon-stimulated genes (Fig. S3A). Bone marrow-derived macrophages (BMDMs) from WT and *Pla2g2e*$^{-/-}$ mice were activated by transfection with poly(I:C) and showed a similar phenotype to that observed *in vivo* (Fig. S3B). The frequency of macrophages in the bronchoalveolar lavage fluids (BALFs) of *Pla2g2e*$^{-/-}$ mice did not exhibit significant differences from that of WT mice on days 3, 7, and 14 p.i. with PR8 virus (Fig. 2C). In contrast, the frequency of neutrophils in the BALFs of *Pla2g2e*$^{-/-}$ mice was significantly lower than that in WT mice on day 3 p.i. but showed no significant difference compared to WT mice on days 7 and 14 p.i. (Fig. 2D). These findings suggest that *Pla2g2e* deficiency does not exert a significant impact on the innate immune response against influenza infections in mice.

Neutralizing antibodies directed against the HA protein are the most established correlate for immunity against influenza, and clearance of influenza viruses is predominantly mediated by neutralizing antibodies (25, 26). We assessed the levels of binding and neutralizing antibodies against PR8 in mouse sera on day 14 p.i. Our findings showed that *Pla2g2e*$^{-/-}$ mice exhibited significantly lower levels of binding antibodies compared to WT mice (Fig. 2E), while no significant difference was observed in neutralizing antibody levels between the two groups (Fig. 2F). Furthermore, we demonstrated that despite the reduction in binding antibody titers in *Pla2g2e*$^{-/-}$ mice, the antibody-dependent cellular cytotoxicity was not significantly altered when compared to WT mice (Fig. 2G). The findings imply that *Pla2g2e* deficiency may not be causally linked to humoral immunity upon influenza virus infection.

Pla2g2e-deficient mice have diminished influenza-specific cellular immunity

T cell-mediated adaptive immune responses play a critical role in conferring protective immunity against influenza virus infection, facilitating viral clearance and promoting host recovery. Given the evidence of delayed viral clearance in *Pla2g2e*$^{-/-}$ mice, we aimed to investigate whether this observation was linked to perturbations in cellular immunity. We first determined the counts of lymphocytes in the BALFs of WT and *Pla2g2e*$^{-/-}$ mice. In response to PR8 challenge, there was a gradual increase in the counts of $CD4^+$ and $CD8^+$ T cells in the BALFs of WT and *Pla2g2e*$^{-/-}$ mice (Fig. 3A and B). On day 7 p.i., the frequencies of $CD4^+$ and $CD8^+$ T cells in the BALFs of *Pla2g2e*$^{-/-}$ mice were lower than those of WT mice. By day 14 p.i., there were no significant differences in the frequencies of $CD4^+$ and $CD8^+$ T cells in the BALFs of two groups (Fig. 3A and B). To characterize influenza antigen-specific T cell immunity in WT and *Pla2g2e*$^{-/-}$ mice, we employed major histocompatibility complex (MHC)-restricted tetramers that recognized the immunodominant I-$A^b$$NP_{311-325}$

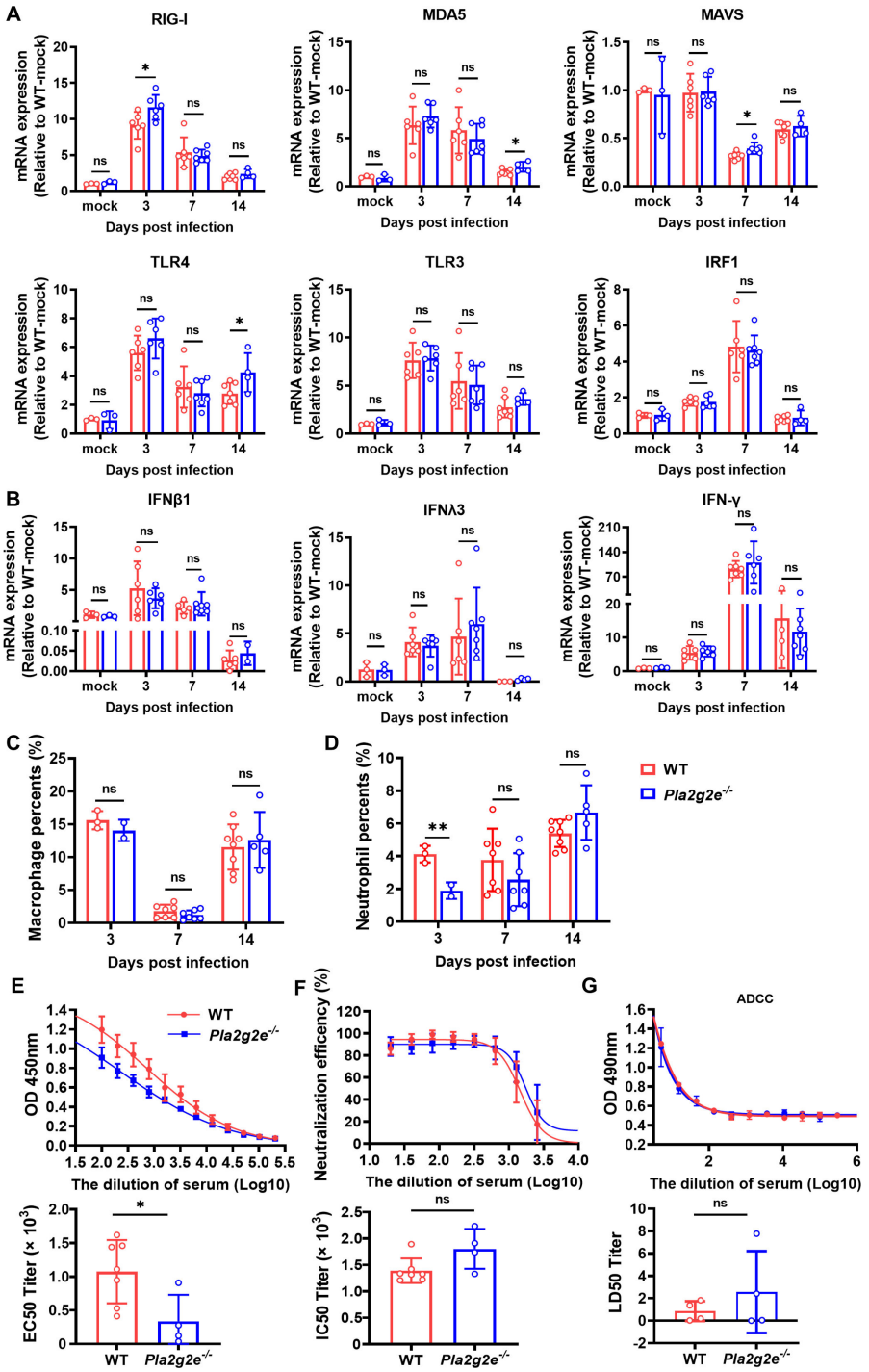

FIG 2 *Pla2g2e*-deficient mice have comparable innate and humoral immune responses to influenza virus challenge. (A–D) WT and *Pla2g2e*$^{-/-}$ mice were infected with 1,000 PFU of PR8 virus and BALFs were collected on days 3 (n = 7), 7 (n = 7), and 14 (n = 8) p.i. (A) The mRNA expression levels of pattern recognition receptors and downstream key regulators in lung tissues of PR8-infected mice on days 3, 7, and 14 p.i. (B) The mRNA expression levels of interferons in lung tissues of PR8-infected mice. The frequencies of alveolar macrophages (C) and neutrophils (D) in BALFs were measured by flow cytometry. (E–G) WT (n = 7) and *Pla2g2e*$^{-/-}$ (n = 4) mice were intranasally infected with 1,500 PFU of PR8 virus. Serum samples were collected on day 14 p.i., and binding antibodies (E) were quantified using an enzyme-linked immunosorbent assay (ELISA), while neutralizing antibodies (F) were measured through a micro-neutralization assay. (G) Antibody-dependent cellular cytotoxicity was measured by the lysis of target cells *in vitro* using a lactate dehydrogenase-release assay in *Pla2g2e*$^{-/-}$ and WT mice. *, $P < 0.05$; **, $P < 0.01$; ns, $P > 0.05$.

CD4 T cell epitope or $D^bNP_{366-374}$ CD8 T cell epitope. Fewer $I\text{-}A^bNP_{311-325}{}^+CD4^+$ T cells and $D^bNP_{366-374}{}^+CD8^+$ T cells were detected in spleen of *Pla2g2e*$^{-/-}$ mice on day 14 p.i. (Fig. S4A and B). Interestingly, there was a decrease in $D^bNP_{366-374}{}^+CD8^+$ T cells present in BALFs of *Pla2g2e*$^{-/-}$ mice compared to WT mice, while an increase in $I\text{-}A^bNP_{311-325}{}^+CD4^+$ T cells was observed (Fig. S4C and D). Activated $CD4^+$ and $CD8^+$ T cells secrete cytokines, including IFN-γ, tumour necrosis factor alpha (TNF-α), and IL-2, to establish an inflammatory microenvironment that facilitates immune cell activation, proliferation, and the development of functional immune cells (27). We further assessed the functionality of $CD4^+$ and $CD8^+$ T cell responses in BALFs and spleens from WT and *Pla2g2e*$^{-/-}$ mice infected with PR8 using an enzyme-linked immunospot assay (ELISpot) and intracellular cytokine staining assay on day 14 p.i. Our findings showed that *Pla2g2e*$^{-/-}$ mice had significantly reduced levels of IFN-γ production in both BALFs and splenic T cells upon stimulation with HA or nucleoprotein (NP peptide pool, compared to the WT group (Fig. 3C and D). Furthermore, the frequencies of IFN-γ^+CD4^+ and IFN-γ^+CD8^+ T cells were significantly lower in *Pla2g2e*$^{-/-}$ mice compared to WT mice, while there were no

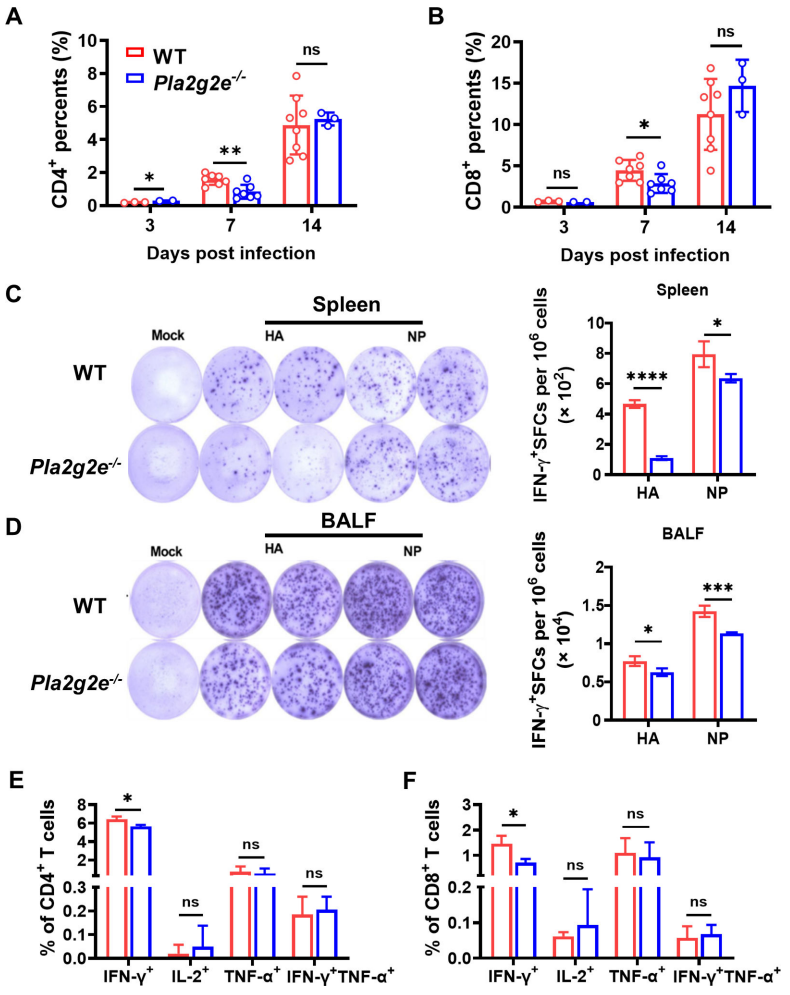

FIG 3 *Pla2g2e*-deficient mice have diminished influenza-specific cellular immunity. (A and B) WT and *Pla2g2e*$^{-/-}$ mice were infected with 1,000 PFU of PR8 virus, and BALFs were collected on days 3 ($n = 7$), 7 ($n = 7$), and 14 ($n = 8$) p.i. The frequencies of alveolar $CD4^+$ T (A), and $CD8^+$ T (B) cells in BALFs were measured by flow cytometry. (C–F) WT ($n = 5$) and *Pla2g2e*$^{-/-}$ ($n = 5$) mice were infected with 1,500 PFU of PR8 virus. On day 14 p.i., BALFs and splenocytes were harvested for subsequent stimulation with pools of HA or NP peptides, respectively. The production of IFN-γ by T cells in BALFs (C) and spleen (D) was evaluated using the ELISpot assay. The functionality of $CD4^+$ (E) and $CD8^+$ (F) T cells was assessed by intracellular cytokines secretion assay. *, $P < 0.05$; **, $P < 0.01$; ***, $P < 0.001$; ****, $P < 0.0001$; ns, $P > 0.05$.

significant differences observed in the production of TNF-α and IL-2 in these T cell subsets (Fig. 3E and F). However, the polyfunctionality (IFN-γ$^+$ and TNF-α$^+$) of both CD4$^+$ and CD8$^+$ T cells was similar between *Pla2g2e*$^{-/-}$ mice and WT mice (Fig. 3E and F). Furthermore, we analyzed the expression of activation marker CD69 in CD8$^+$ T cells and observed no significant difference in the proportion of CD69$^+$CD8$^+$ T cells between the two groups (Fig. S4E). We also investigated the expression of chemokine receptors involved in T-lymphocyte migration to the infection site and demonstrated a significant decrease in CCR5, CCR7, and CCR8 expression in T cells present in the BALFs of *Pla2g2e*$^{-/-}$ mice compared to WT mice (Fig. S4F). These findings suggest that *Pla2g2e*$^{-/-}$ mice exhibit delayed recruitment of T cells and perturbed development of functional T cell immunity.

Pla2g2e deficiency reduces influenza-specific T cell-mediated cytotoxicity

After antigen receptor-mediated activation, CD8$^+$ T cells undergo proliferation and differentiation into effector cells that are capable of eliminating infected cells and conferring protection against infections. The effector mechanisms employed by cytotoxic T lymphocytes to eliminate target cells involve the secretion of death-inducing effector molecules, notably granzymes, perforin, and Fas-ligand (28). *Pla2g2e*$^{-/-}$ mice had a significant decrease in granzyme B secretion in CD8$^+$ T cells upon exposure to HA and NP peptide pool (Fig. 4A). Additionally, *Pla2g2e* deficiency resulted in significantly impaired cytotoxicity mediated by CD8$^+$ T cells both *in vitro* and *in vivo* (Fig. 4B and C). These findings suggest that *Pla2g2e* deficiency results in reduced cytotoxicity mediated by influenza-specific T cells.

Transgenic mice expressing human *PLA2G2E* gene exhibit resistance to influenza virus infection

To confirm the anti-influenza effects of PLA2G2E, we generated a transgenic mouse model with systemic expression of human *PLA2G2E* gene at *Rosa26* genomic safe harbor site, designated as *hPLA2G2E* mice. Eight-week-old *hPLA2G2E* mice were inoculated with 2,000 PFU of PR8 virus, and their body weight and survival rate were monitored for 14 days. The *hPLA2G2E* mice exhibited a significantly slower rate of weight loss compared to that of WT mice (Fig. 5A). On day 10 p.i., the weight loss in WT mice exceeded 30%, meeting the endpoint criteria for mortality, while the weight of *hPLA2G2E* mice began to recover and gradually returned to pre-infection levels (Fig. 5A). Moreover, *hPLA2G2E* mice showed a survival rate exceeding 60%, whereas all WT mice succumbed to infection (Fig. 5B). In terms of influenza-specific immune response analysis in spleen cells from these two groups, there was a significant increase in the frequencies of D^{b}NP$_{366\text{-}374}$$^+$CD8$^+$ T cells in *hPLA2G2E* mice compared to WT mice, while there was no significant difference observed in I-A^{b}NP$_{311\text{-}325}$$^+$CD4$^+$ T cells (Fig. S5A and B). Additionally, upon stimulation with HA or NP peptide pool, both BALFs and splenic T cells from *hPLA2G2E* mice had significantly increased levels of IFN-γ production compared to those from WT mice (Fig. 5C and D). Intracellular cytokine staining analysis revealed a significantly higher frequency of IFN-γ$^+$CD4$^+$, IFN-γ$^+$CD8$^+$, and TNF-α$^+$CD8$^+$ cells in *hPLA2G2E* mice compared to WT mice (Fig. 5E and F). Furthermore, there was a marked increase in the polyfunctionality (IFN-γ$^+$ and TNF-α$^+$) of CD8$^+$ T cells (Fig. 5F). However, the frequencies of IL-2$^+$CD4$^+$ and IL-2$^+$CD8$^+$ T cells were significantly diminished in *hPLA2G2E* mice, indicating a reduction in IL-2 production within PR8-specific T cells, which could decrease the proliferation of T and B lymphocytes. The *hPLA2G2E* mice also had a significantly higher killing capacity and granzyme B production of CD8$^+$ T cells compared to WT mice (Fig. 5H and I). In addition, *hPLA2G2E* mice exhibited slightly higher levels of binding antibodies compared to WT mice (Fig. S5C), while no significant difference was observed in neutralizing antibody levels (Fig. S5D) and antibody-dependent cellular cytotoxicity (Fig. S5E) between the two groups. These findings suggest that PLA2G2E confers protection against mortality associated with influenza virus infection and enhances influenza-specific cellular immunity in *hPLA2G2E* mice.

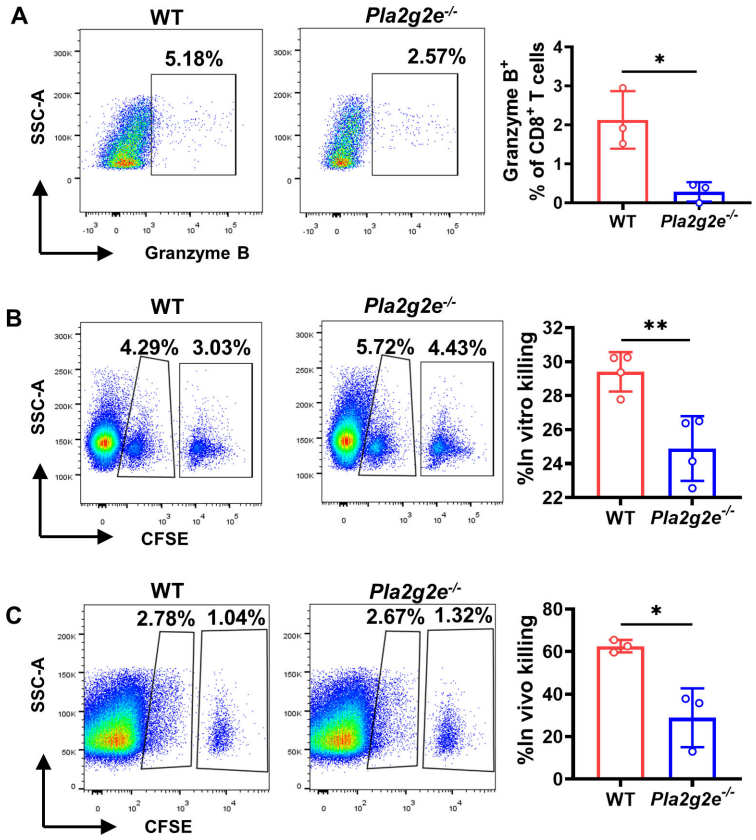

FIG 4 *Pla2g2e* deficiency reduces influenza-specific T cell-mediated cytotoxicity. (A–C) WT (n = 7) and *Pla2g2e*$^{-/-}$ (n = 6) mice were infected with 1,500 PFU of PR8 virus, and splenocytes were collected on day 14 p.i. (A) The frequencies of PR8-specific CD8^{+}granzyme B^{+} T cells were detected using flow cytometry, following stimulation with a pool of HA and NP peptides. (B) *In vitro* influenza-specific splenic T cell-mediated cytotoxicity from WT and *Pla2g2e*$^{-/-}$ mice. (C) *In vivo* influenza-specific splenic T cell-mediated cytotoxicity in WT and *Pla2g2e*$^{-/-}$ mice. *, $P < 0.05$; **, $P < 0.01$.

Pla2g2e deficiency results in the alteration of lipid mediators in the lung and T cells of infected mice

sPLA2 plays an important role in the production of lipid mediators, which are crucial regulators of inflammation and key contributors to the pathogenesis of influenza (29). We performed mass spectrometry-based lipidomic analysis of eicosanoids in lung tissues and isolated T cells from both *Pla2g2e*$^{-/-}$ and wild-type mice on day 7 p.i. A total of 55 and 56 lipid metabolites were detected and quantified in lung tissues and isolated T cells, respectively. The levels of FFA14:0, 13-Hydroxyoctadecadienoic acid (13-HODE), and dhk-PGE2 (P = 0.051) were decreased in lungs of uninfected *Pla2g2e*$^{-/-}$ mice, while 4-HDHA and 17,18-diHETE were increased (Fig. S6A). The lungs of PR8-infected WT mice exhibited upregulation of a total of 20 lipid metabolites, including polyunsaturated fatty acids, lipoxygenase products, and DHA metabolites, compared to their phosphate-buffered saline (PBS)-treated counterparts (Fig. S6B). Furthermore, the levels of most lipid metabolites in the lungs of PR8-infected *Pla2g2e*$^{-/-}$ mice were significantly higher compared to those observed in PBS-treated *Pla2g2e*$^{-/-}$ mice or PR8-infected WT mice (Fig. 6A). Surprisingly, we only observed a significant upregulation of FFA18:1 and FFA22:6, along with a notable downregulation of prostaglandin D2 (PGD2) and 15d-PGJ2 in the purified T cells of PR8-infected *Pla2g2e*$^{-/-}$ mice compared to PR8-infected WT mice (Fig. 6B; Fig. S6C). *Pla2g2e* deficiency leads to the accumulation of arachidonic acid-derived lipid mediators in the lung of infected mice, while concurrently reducing specific lipid

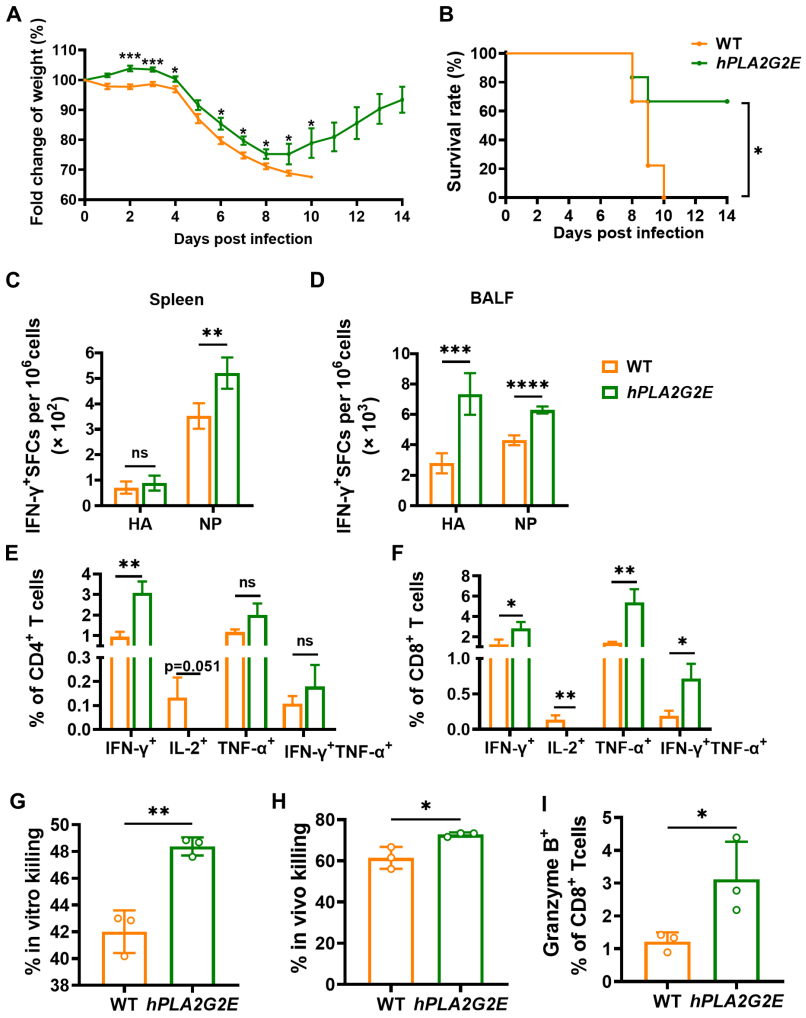

FIG 5 The transgenic mice expressing human *PLA2G2E* gene exhibit resistance to influenza virus infection. (A–F) WT (n = 8) and *hPLA2G2E* (n = 6) mice were intranasally infected with 2,000 PFU of PR8 virus. (A and B) Body weight (A) and survival (B) of PR8-infected mice were monitored daily for 14 days. (C and D) On day 14 p.i., BALFs and splenocytes were harvested for subsequent stimulation with pools of HA or NP peptides, respectively. The production of IFN-γ by T cells in spleen (C) and BALFs (D) was evaluated using the ELISpot assay. The functionality of $CD4^+$ (E) and $CD8^+$ (F) T cells were assessed by intracellular cytokines secretion assay. (G) *In vitro* influenza-specific splenic T cell-mediated cytotoxicity from WT and *hPLA2G2E* mice. (H) *In vivo* influenza-specific splenic T cell-mediated cytotoxicity in WT and *hPLA2G2E* mice. (I) The frequencies of PR8-specific splenic $CD8^+$granzyme B^+ T cells were detected using flow cytometry, following stimulation with a pool of HA and NP peptides. *, $P < 0.05$; **, $P < 0.01$; ***, $P < 0.001$; ****, $P < 0.0001$; ns, $P > 0.05$.

mediators in T cells. This phenomenon may contribute to delayed recruitment of T cells and perturbed development of functional T cell immunity associated with *Pla2g2e* deficiency.

Pla2g2e deficiency does not influence gut microbiome shaping

Gut microbiota plays a crucial role in regulating immune responses at distant mucosal sites, particularly in the lungs (30). sPLA2 contributes to shaping gut microbiota, which can impact distal tissue phenotypes (31, 32). The expression of PLA2G2E in the colon (33) raises the question of whether it modulates pulmonary immune responses through remodeling of gut microbiota. To investigate this, we co-housed *Pla2g2e*$^{-/-}$ and WT mice

for 14 days and inoculated them with 1,500 PFU of PR8 virus. On day 14 p.i. co-housed *Pla2g2e*$^{-/-}$ mice exhibited significantly reduced levels of IFN-γ production in T cells both in BALFs and spleen upon stimulation with HA or NP peptide pool, compared to the WT group (Fig. 6C and D). These observations were consistent with those observed in independently reared *Pla2g2e*$^{-/-}$ mice (Fig. 3C and D). These findings suggest that PLA2G2E regulates anti-influenza immune responses independent of its influence on gut microbiota shaping.

DISCUSSION

It is clear that the various secreted phospholipases can have isoform-specific and tissue-specific effects. Therefore, the role of sPLA2 isoforms in respiratory virus infection requires further investigation. PLA2G2E is expressed at low levels in multiple tissues (18) and is induced in lung epithelial cells and alveolar macrophages after influenza virus infection (21–23). Our study confirmed the upregulation of PLA2G2E in the lungs of

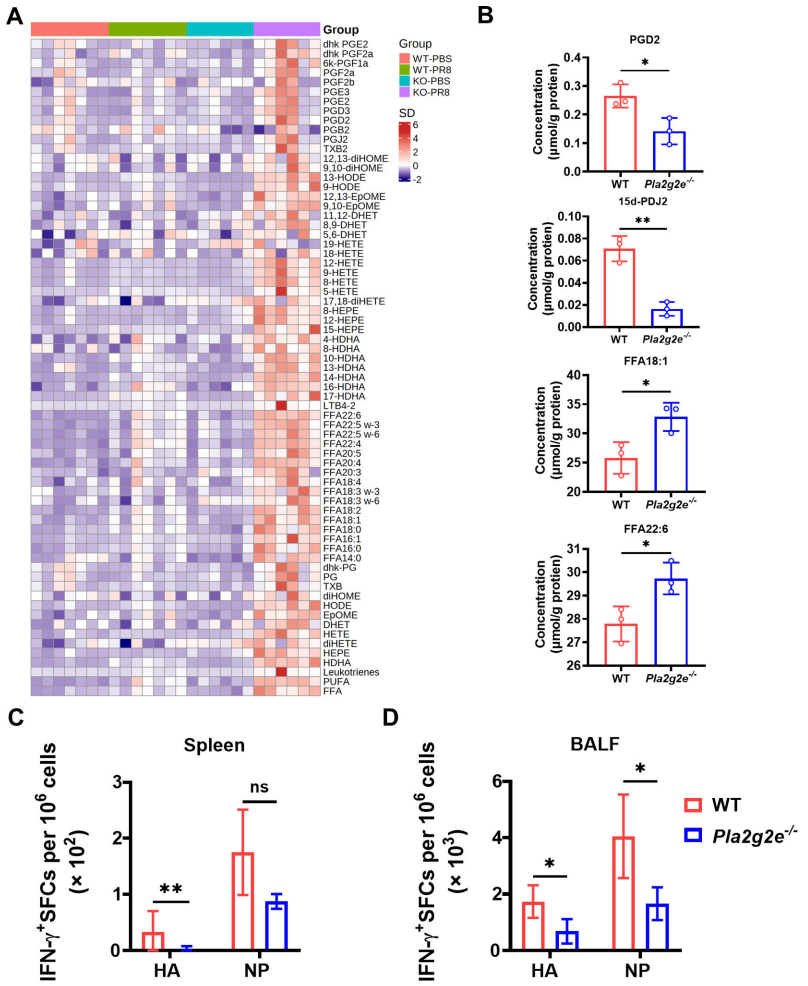

FIG 6 *Pla2g2e* deficiency results in the accumulation of arachidonic acid-derived lipid mediators in the lung of infected mice, while reducing certain lipid mediators in T cells. (A and B) WT and *Pla2g2e*$^{-/-}$ mice were infected with 1,500 PFU of PR8 virus, lungs and splenocytes were harvested on day 7 p.i. for subsequent mass spectrometry-based lipidomic analysis, n = 6–7 per group. (A) Heatmaps of lipid mediators in lung tissues of each group. (B) The levels of PGD2, 15d-PDJ2, FFA18:1, and FFA22:6 in CD3$^+$ T cells of WT and *Pla2g2e*$^{-/-}$ mice. (C and D) WT (n = 6) and *Pla2g2e*$^{-/-}$ (n = 6) mice were infected with 1,500 PFU of PR8 virus after co-housing for 14 days. On day 14 p.i., BALFs and splenocytes were harvested for subsequent stimulation with pools of HA or NP peptides, respectively. The production of IFN-γ by T cells in spleen (C) and BALF (D) was evaluated using the ELISpot assay. *, $P < 0.05$; **, $P < 0.01$; ns, $P > 0.05$.

mice infected with H1N1 A/Puerto Rico/8/1934 virus and investigated its role during infection using a targeted mouse model lacking *Pla2g2e* gene (*Pla2g2e*$^{-/-}$). Our findings demonstrated that *Pla2g2e*$^{-/-}$ mice exhibited lower survival rates and higher viral loads in their lungs compared to wild-type mice following influenza virus infection. While *Pla2g2e*$^{-/-}$ mice displayed comparable innate and humoral immune responses to influenza virus challenge, they showed impaired influenza-specific cellular immunity and reduced T cell-mediated cytotoxicity. Furthermore, transgenic mice expressing the human *PLA2G2E* gene exhibited resistance to influenza virus infection along with enhanced influenza-specific cellular immunity and T cell-mediated cytotoxicity. Notably, *hPLA2G2E* mice demonstrated a significant enhancement in CD8$^+$ T cell polyfunctionality. Our work supports further investigation of the therapeutic potential of enhancing PLA2G2E during influenza virus infection as well as the interplay between PLA2G2E and adaptive immunity.

Two additional sPLA2 enzymes, PLA2G2D and PLA2G10, are found to be upregulated in the lungs of mice infected with influenza virus and are implicated in exacerbating outcomes in mice infected with influenza virus (34, 35). Aged *Pla2g2d*$^{-/-}$ mice exhibit robust protection against lung injury following infection with influenza virus (34). The absence of PLA2G2D leads to a reduction in airway levels of anti-inflammatory PGD2, thereby promoting pulmonary dendritic cell migration into lymph nodes, enhancing antiviral CD4$^+$ and CD8$^+$ T cell responses, mitigating lung damage, and improving survival (15, 34). The involvement of PLA2G10 and its downstream products in the inhibition of adaptive immunity during influenza virus infection in mice may contribute to pathogenesis. It is plausible that T and B cell maturation and activation are initiated in mice lacking *PLA2G10* prior to virus infection, potentially leading to an earlier and more robust adaptive immune response that enhance the survival of *Pla2g10*$^{-/-}$ mice after H1N1 infection (35). The present study, in contrast, demonstrated that PLA2G2E was also induced by influenza virus infection and conferred protection against influenza virus infection through the enhancement of influenza-specific cellular immunity and T cell-mediated cytotoxicity. Classical sPLA2s (group I/II/V/X) are closely related enzymes with highly conserved His/Asp catalytic dyad. However, they serve distinct roles in the context of influenza virus infection. One potential mechanism is that individual sPLA2s exhibit distinct substrate selectivity. In terms of the sn-2 fatty acids, PLA2G2E releases various fatty acids in a non-selective manner, while PLA2G2D and PLA2G10 demonstrate varying degrees of preference for polyunsaturated fatty acids (14). On the other hand, sPLA2s exhibit non-enzymatic functions and play pivotal roles in a wide range of physiological processes. Administration of PLA2G2D-Fc fusion protein enhances Treg cells while also limiting colitis and experimental autoimmune encephalomyelitis in mice, and this immunosuppressive effect is independent of its enzymatic activity (36). Catalytically inactive PLA2G12B, primarily expressed in the liver and induced by hepatocyte nuclear factor 4 alpha (HNF4α) and estrogen-related receptor gamma (ERRγ) transcription factors, is believed to regulate very low-density lipoprotein (VLDL) secretion from hepatocytes (37, 38). Presumably, there may exist receptor-like proteins that bind to the enzymatic activity-independent sPLA2s for signal transduction or chaperone-like proteins that collaborate with these sPLA2s to exert their physiological functions.

Bioactive lipid mediators, are crucial regulators of inflammation and key contributors to the pathogenesis of influenza (29). PGD2 and its metabolites are multifaceted mediators, through its interaction with the chemoattractant receptor-homologous molecule expressed on Th2 cells (CRTH2) receptor on T cells, that significantly influences T cell function, including recruitment and migration, differentiation, cytokine production, and survival (39). Our study demonstrated a significant decrease in PGD2 and 15d-PGJ2 production in the purified T cells of PR8-infected *Pla2g2e*$^{-/-}$ mice, which may contribute to *Pla2g2e* deficiency leading to delayed recruitment of T cells and perturbed development of functional T cell immunity. 13-HODE exhibits chemotactic activity toward neutrophils (40) and is reduced in uninfected *Pla2g2e*$^{-/-}$ mice, potentially contributing to the significantly decreased initial phase of neutrophil infiltration in these mice. In

contrast, *Pla2g2e* deficiency resulted in the accumulation of arachidonic acid-derived lipid mediators in the lung of PR8-infected mice. However, the effects of elevated lipid mediators on the pathogenesis of influenza infection and the T cell immune response need to be further studied.

Host lipid metabolism orchestrates the subcellular localization of key events in the viral life cycle. The sensitivity to hydrolysis of phospholipids by sPLA2 enzymes has been reported to differ depending on the lipid composition and overall structure (14). The sPLA2s derived from snake venom have been reported to exhibit potent virucidal activity against hepatitis C virus (HCV), Dengue virus (DENV), Japanese encephalitis virus (JEV), and YFV, which belong to the *Flaviviridae* family and bud through the endoplasmic reticulum (41–43). Additionally, human sPLA2 PLA2G10 demonstrates virucidal activity against human immunodeficiency virus (HIV) (44), which is known to bud through the plasma membrane. The phospholipid contents of the endoplasmic reticulum membranes differ from those of the plasma membranes. This activity is achieved by disrupting the lipid bilayers of viral envelopes. In addition, sPLA2s obtained from the venom of bees and snakes were reported to inhibit the entry of HIV into host cells without disrupting the viral envelope (45). PLA2G12B is required in the late stage of the HCV life cycle and the PLA2G12B-mediated VLDL secretory pathway is important for HCV assembly and secretion (46). The results of our study indicate that there were no differences in the lung viral RNA loads between *Pla2g2e*$^{-/-}$ mice and wild-type mice during the early stages of infection. However, on days 7 and 10 p.i., the viral RNA loads in *Pla2g2e*$^{-/-}$ mice were significantly higher than those observed in WT mice. These findings suggest a less efficient clearance of influenza virus in *Pla2g2e*$^{-/-}$ mice compared to their WT counterparts, rather than a lack of PLA2G2E-mediated virucidal activity against influenza virus.

In summary, our findings offer novel insights into the molecular pathophysiology of influenza virus infection, highlighting a previously unrecognized role for PLA2G2E in the context of influenza virus infection. Our results demonstrate that PLA2G2E does not impact innate and humoral immune responses to influenza virus challenge but rather modulates influenza-specific cellular immunity and T cell-mediated cytotoxicity. Further investigations will aim to unravel the underlying mechanisms driving this observed phenotype.

MATERIALS AND METHODS

Cell culture

HEK293T, MDCK, Hela, A549, and NCI-H1299 cell lines were obtained from the National Collection of Authenticated Cell Cultures in Shanghai, China, and were maintained in complete Dulbecco's Modified Eagle Medium (DMEM, Gibco) supplemented with 10% (vol/vol) heat-inactivated fetal bovine serum (Gibco), L-glutamine (2 mM, Gibco), and penicillin-streptomycin (100 U/mL, Gibco).

Influenza virus propagation and purification

The mouse-adapted strain of influenza virus H1N1 A/Puerto Rico/8/34 (PR8) was rescued by co-transfection with eight-plasmid PR8 virus rescue system in HEK293T cells. Forty-eight hours after transfection, culture supernatants were inoculated into 10-day-old embryonated chicken eggs. Two days later, progeny viruses were harvested from the allantoic fluid and clarified by centrifugation at 6,000 r.p.m. at 4°C for 15 min using a Beckman rotor SW28. The clarified supernatants were subsequently layered onto a cushion of sucrose (30% wt/vol) and further centrifuged at 25,000 r.p.m. for 2.5 h. The purified viruses were suspended in PBS buffer supplemented with 0.5% bovine serum albumin (BSA, Sigma-Aldrich) and stored at −80°C for long-term preservation.

Mice and administration

Pla2g2e$^{-/-}$ and human *PLA2G2E* transgenic (*hPLA2G2E*) mice were purchased from Cyagen Biosciences (Suzhou, China) and were housed in a specific pathogen-free facility on a 12-h dark/light cycle and fed a standard diet. The pups were genotyped by PCR analysis followed by sequencing analysis. For co-housing experiment, cohousing female WT and *Pla2g2e*$^{-/-}$ mice for a duration of 14 days facilitated the transfer of gut microbiota via coprophagy.

The 8- to 12-week-old female *Pla2g2e*$^{-/-}$ and *hPLA2G2E* mice were anesthetized with isoflurane prior to intranasal inoculation of the PR8 influenza virus. The viral dose used was either 1,500 or 2,000 PFU in 40 µL of PBS. Littermate wild-type mice were used as controls. Animals were monitored daily for survival and weight change. The achievement of a weight loss exceeding 30% will meet the endpoint criteria for mortality.

Lung viral titration

Lung viral loads were titrated by plaque formation assay. Lung tissues from PR8-infected mice at 3, 7, and 10 d.p.i. were harvested and then homogenized with PBS. Confluent MDCK cell monolayers in six-well plates were infected with 10- to 1,000-fold dilution of supernatants of lung homogenate for 2 h. The supernatants were aspirated and washed twice with PBS to remove residual virus. Each well was subsequently covered with an agar overlay containing 0.6% agar, 1 × Minimum Essential Medium (MEM) (Gibco), 0.4% BSA, 1% penicillin-streptomycin (PS), and 1 µg/mL L-1-tosylamido-2-phenylethyl chloromethyl ketone (TPCK)-Trypsin (Sigma) and incubated at 37°C with 5% CO_2 for 4 days. The overlays were carefully removed and cells were fixed with 4% formaldehyde (GenXion Biotechnology) for 20 min and stained with 0.2% crystal violet (Yeasen) for 20 min. Plaques were counted for the calculation of viral titers as PFU per gram of lung tissue.

Histopathological analysis

Lung tissues harvested from mock and PR8-infected mice at 3, 7, and 10 d.p.i. were fixed in 4% formaldehyde and embedded in paraffin. Lung sections were stained with H&E (Servicebio) and examined for histopathological changes. Images were acquired using a Panoramic slice scanner.

Bronchoalveolar lavage

The trachea was exposed via a midline incision and cannulated using a sterile 18G intravenous catheter (Vasofix, Braun). Bronchoalveolar lavage was performed by instilling four 0.8 mL PBS into the lung. The collected BALFs were centrifuged at 500 × *g* for 5 min. The supernatants were collected, and the BALF cells were lysed with a red cell lysis solution. The total cell numbers were counted and then stained for flow cytometry analysis.

Flow cytometry analysis

The following monoclonal antibodies were used for flow cytometry analysis: PerCP-Cyanine5.5 conjugated anti-CD45 Mab (clone: 30-F11, BD Biosciences), Biotin conjugated anti-CD103 Mab (clone: 2E7, BioLegend), APC conjugated anti-CD8α Mab (clone: 53-6.7, BD Biosciences), PE conjugated anti-CD69 Mab (clone: H1.2F3, eBioscience), Brilliant Violet 421 conjugated anti-CD3 Mab (clone: 145-2C11, BioLegend), APC-Cy7 conjugated anti-CD4 Mab (clone: RM4-5, BD Biosciences), FITC Streptavidin (BD Biosciences), Biotin conjugated anti-CD45 Mab (clone:30-F11, BioLegend), APC-eFluor 780 conjugated anti-CD11b Mab (clone: M1/70, eBioscience), PerCP-Cyanine5.5 conjugated anti-Ly6G/Ly6C Mab (clone: RB6-8C5, eBioscience), eFluor 450 conjugated anti-CD11c Mab (clone: N418, eBioscience), PE conjugated anti-F4/80 Mab (clone: T45-2342, BD Biosciences), PE conjugated anti-Granzyme B Mab (clone: NGZB, eBioscience), PE-Cy7 conjugated

anti-TNF Mab (clone: MP6-XT22, BD Biosciences), PE conjugated anti-IL-2 Mab (clone: JES6-5H4, BD Biosciences), FITC conjugated anti-IFNγ Mab (clone: XMG1.2, eBioscience).

For intracellular cytokines staining, cells were fixed and permeabilized using Cytofix/Cytoperm Solution (BD Biosciences) after washing and stained with the cytokine antibodies. To detect antigen-specific T cells after influenza A virus (IAV) infection, 1×10^6 cells were cultured in 96-well round bottom plates in the presence of 10 µg/mL Brefeldin A (Invitrogen) at 37°C for 4 h and stimulated with pools of HA and NP peptide for 24 h.

For cell markers and tetramers staining, 1×10^6 cells were blocked with 1 µg anti-CD16/32 antibody (clone: 93, BioLegend) and stained with cell markers or PE-conjugated I-$A^b NP_{311\text{-}325}$ tetramers (Proimmune) and APC-conjugated $D^b NP_{366\text{-}374}$ tetramers (HELIXGEN) at room temperature for 1 h. The stained cells were detected with an LSR Fortessa flow cytometer (BD, USA) and analyzed using FlowJo software (Tree Star).

ELISA

The binding IgG antibodies in the sera of PR8-infected mice were measured by ELISA. Ninety-six-well plates were coated with 0.1 µg total proteins of inactivated PR8 virus and incubated overnight at 4°C. Subsequently, the plates were blocked with PBST (PBS supplemented with 0.1% Tween-20) and 5% skim milk (Beyotime Biotechnology) for 2 h at 37°C. Serially diluted serum samples ranging from 1:100 to 1:204,800 were added to each well, followed by incubation for 1 h at 37°C. Horseradish peroxidase (HRP)-conjugated goat anti-mouse antibody (diluted to a concentration of 1:2,000 in PBS containing 5% skim milk, Beyotime Biotechnology) was then added to the wells and allowed to incubate for another hour at 37°C. The reaction was developed using a tetramethylbenzidine (TMB, Millipore) substrate and measured spectrophotometrically at a wavelength of absorbance equal to or greater than 450 nm. Background readings were obtained by including control wells filled with PBS. The endpoint titer was defined as the reciprocal of the highest serum dilution that yielded a signal twofold higher than the background.

Microneutralization assay

MDCK cells were seeded in 96-well plates at a density of 2.5×10^4 cells per well and incubated at 37°C for 18–20 h. Twenty-five microliters of mouse serum sample was mixed with three times volume of receptor-destroying enzyme (Sigma-Aldrich) and digested in water bath at 37°C for 16–18 h. After heat inactivation of serum at 56°C for 30 min, serum was serially diluted twofold from a starting dilution of 1:10 to a final dilution of 1:1,250. An equal volume of virus at a concentration of 100 50% tissue culture infectious dose (TCID50)/well was mixed with serum and incubated at 37°C for 1 h. The MDCK cells were washed twice with PBS before transferring the serum-virus mixture onto them, which was then incubated at 37°C for 2 h. The mixtures were then replaced with DMEM supplemented with 0.4% BSA and 1 µg/mL TPCK for an additional 48 h. The supernatants were discarded and cells were fixed with 80% acetone at room temperature for 15 min. The plates were blocked with 1× PBST supplemented with 5% skim milk for 2 h at 37°C. The wells were incubated with pan-Nucleoprotein rabbit Mab (Sino Biological) at a dilution of 1:1,000 in PBS at 37°C for 1 h and then with HRP-conjugated goat anti-rabbit (1:2,000, Beyotime Biotechnology) for another 1 h. The reaction was developed by TMB substrate and determined at 450 nm. Wells containing only PR8 were utilized as a negative control, while wells lacking serum and PR8 served as the blank control. Cell viability was calculated using the formula: $1 - ([OD_{serum} - OD_{blank}] / [OD_{control} - OD_{blank}]) \times 100\%$.

Antibody-dependent cell-mediated cytotoxicity

The antibody-dependent cellular cytotoxicity (ADCC) assay was modified from a previously described method (47). Briefly, 2.5×10^6 Hela cells were seeded in six-well plates and transfected with PR8-HA plasmids. Two days after transfection, Hela cells were seeded at a density of 4×10^4 per well in 96-well plates and used as target cells. Sera

from PR8-infected WT and *Pla2g2e*$^{-/-}$ mice were diluted in 96 wells in a threefold serial dilution from a starting dilution of 1:5 to a final dilution of 1: 295,245. Splenocytes were isolated from WT mice and pre-incubated with the sera and incubated at 37°C for 1 h. In addition, 4×10^5 splenocytes were added to the target cells and incubated at 37°C for 6 h. Finally, the release of lactate dehydrogenase (LDH) was measured using an LDH cytotoxicity assay kit (Yeasen, China) as a surrogate marker of target cell lysis. The optical density values were measured at 490 nm using the Synergy HT multi-mode microplate reader from BioTek Instruments.

CD8$^+$ T cells separation

Single-cell suspensions of splenocytes were prepared from mock and PR8-infected mice. CD8$^+$ T cells were purified through a two-step process. Briefly, splenocytes were positively selected using CD8a (Ly-2) MicroBeads (Miltenyi Biotec) and subsequently isolated using LS Separation columns (Miltenyi Biotec) following the manufacture's instruction.

In vivo cytotoxicity assay

In vivo T cell-mediated cytotoxicity assay was performed as described previously (48). In brief, splenocytes from uninfected WT mice were stained with high 10 µM, carboxyfluorescein succinimidyl ester (CFSE^{high}) or low (1 µM, CFSE^{low}) concentrations of CFSE (Molecular Probes) at 37°C for 15 min. CFSE^{high} cells were then pulsed with HA and NP peptide pool (10 µg/mL) at 37°C for 1 h. A total of 5×10^5 cells from each group (CFSE^{high} and CFSE^{low}) was mixed (10^6 cells total) and transferred i.v. into *Pla2g2e*$^{-/-}$ and WT mice at 14 d.p.i. Spleens were harvested 16 h later and analyzed for numbers of CFSE^{high} and CFSE^{low} cells. The percentage of specific killing was calculated using the following formula: 1 – ([% peptide pulsed in infected/% unpulsed in infected] / [% peptide pulsed in uninfected/% unpulsed in uninfected]) × 100%.

In vitro cytotoxicity assay

Effector cells (splenocytes from PR8-infected WT and *Pla2g2e*$^{-/-}$ or *hPLA2G2E* mice) were suspended at a final concentration of 2.5×10^6 cells/mL. Target cells (splenocytes from uninfected WT mice) were stained with high (10 µM, CFSE^{high}) or low (1 µM, CFSE^{low}) concentrations of CFSE at 37°C for 15 min. Subsequently, CFSE^{high} cells were pulsed with pools of HA or NP peptides (10 µg/mL) for 1 h at 37°C. The cells from each group (CFSE^{high} and CFSE^{low}) were harvested after washing once and were adjusted to 1.0×10^5 cells/mL. The cells were placed into a well of 24-well plate at an appropriate effector:target ratio (25:1:1) and incubated for 6 h at 37°C. The stained cells were harvested and detected with an LSR Fortessa flow cytometer (BD, USA) and were analyzed using FlowJo software (Tree Star). Percentage of cell killing was calculated using the following formula: 1 – (% peptide pulsed in infected / % unpulsed in infected) × 100%.

ELISpot assay

ELISpot assay (Mouse IFN-γ ELISpot kit; U-CyTech) was used to determine specific T cell immune responses to influenza infection. IFN-γ ELISpot assays were performed using freshly isolated mouse splenic lymphocytes or BALFs. A sterile 96-well microtiter plate (Merck Millipore) was coated with anti-mouse IFN-γ capture antibody at 4°C overnight. Single-cell suspensions of splenocytes and BALFs were obtained from PR8-infected mice and seeded onto antibody-coated plates at a concentration of 2×10^5 cells/well or 2.5×10^4 cells/well, respectively. Cells were stimulated with or without 2 µg/mL HA or NP peptides for 24 h at 37°C and then discarded. The plate was then incubated with biotin-conjugated anti-IFN-γ detection antibody (U-CyTech) at 4°C for 16 h, followed by incubation with alkaline phosphatase-conjugated streptavidin (BD Biosciences) at 37°C for 2 h. The nitro blue tetrazolium (NBT)/5-bromo-4-chloro-3-indolyl phosphate (BCIP)

(Thermo Fisher) was added as a substrate for cytokine spot detection. Spots were imaged and quantified with a CTL ImmunoSpot Analyzer (Cellular Technology Ltd, USA).

BMDMs isolation

WT and *Pla2g2e*$^{-/-}$ mice were euthanized and the hind legs were removed. The flesh and muscles adhering to the bones were dissected using sterile scissors and forceps. Epiphyses of femur and tibia were removed, so that the bone marrow can be accessed from the ends with a 23G needle. Bone marrows were washed into a 50 mL tube by gently injecting 2–3 mL cold PBS per bone, passed through a 70 µm Nylon cell strainer to exclude solid particles. The filtrate was centrifuged at 450 × *g* for 10 min at 4°C. Then, the pellet was suspended in 4 mL red blood cell lysis buffer for 30 s to break up red blood cell, and added 10 mL ice-cold, complete DMEM afterward. Subsequently, cells were distributed into dish at 4×10^5 per dish (Greiner), and added 20 ng/mL M-CSF (Sino Biological) to cells and incubated for 7 days. BMDMs were harvested and seeded into plates, and then transfected with poly(I:C) (Invivogen) at a dose of 100 µg or 500 µg per well for 24 h.

RNA isolation and quantitative real-time PCR

Total RNA was extracted from A549, NCI-H1299, and lung tissues of mock or PR8-infected mice at the different time points p.i. using TRIzol reagent (Life Technologies). One microgram of total RNA was used for cDNA synthesis using the HiScript II Q RT SuperMix for qPCR (+gDNA wiper) (Vazyme, China). All reactions were performed with 2× SYBR Green Master Mix (Bio-Rad). on a CFX96 real-time quantitative PCR instrument (Bio-Rad) Gene expression was normalized to the housekeeping gene hypoxanthine phosphoribosyltransferase. The primers were shown in Table S1.

Viral loads in lung tissues were quantified using absolute quantitative RT- PCR. PR8 NA plasmid standard, with a concentration gradient dilution of 10-fold (10^8 copies/µL, 10^7 copies/µL, 10^6 copies/µL, 10^5 copies/µL, 10^4 copies/µL, 10^3 copies/µL, 10^2 copies/µL, 10^1 copies/µL), was employed as the DNA template for this study. The viral loads were calculated as the genome copies of PR8 in 1 µg RNA.

Lipidomic profiling

Eicosanoids in samples were quantitated at LipidALL Technologies as previously described (49). One hundred milligrams of lung tissue or 5×10^6 T cells were extracted in a buffer comprising methanol containing 0.1% (wt/vol) of butylated hydroxytoluene and butylated hydroxyanisole with formic acid and internal standard cocktail added. Samples were vortexed to allow thorough mixing. A fixed amount of ceramic beads pre-cleaned with methanol was then added and the cell samples were incubated at 1,500 rpm for 12 h at 4°C to ensure efficient extraction of eicosanoids from the cell matrix. The samples were centrifuged at 4°C for 10 min at 12,000 rpm, and the supernatant was extracted. The extraction was repeated for a second round. The pooled supernatants were enriched for eicosanoids via solid phase extraction (SPE) using Oasis Prime HLB columns (30 mg, Waters, USA) as previously described (50). The internal standard cocktail contained PGD2-d4, PGE2-d4, PGF2a-d4, 15-deoxy-D12,14-prostaglandin J2-d4, 6-keto-PGF1a-d4, 13,14-dihydro-15-keto prostaglandin F2a-d4, thromboxane B2-d4, HETE:5(S)-hydroxy-eicosatetraenoic acid-d8, HETE:12(S)-hydroxy-eicosatetraenoic acid-d8, HETE:15(S)-hydroxy-eicosatetraenoic acid-d8, HETE: 20-hydroxy arachidonic acid-d6, DiHOME: 9,10-dihydroxy octadecenoic acid-d4, DiHOME: 12,13-dihydroxy octadecenoic acid-d4, leukotriene B4-d4, HODE: 9(S)-hydroxy-octadecadienoic acid-d4, HODE: 13(S)-hydroxy-octadecadienoic acid-d4, ARA-d11, d31-16:0, EOME: 9,10-EOME-d4, EOME: 12,13-EOME-d4, DHET:11,12-DHET-d10, 5-iso prostaglandin F2a VI-d11 in methanol (Cayman chemicals, USA). SPE eluents were transferred to tubes containing 20 µL of ethanol:glycerol, 1:1 (vol/vol), to prevent complete desiccation, and dried under flowing stream of nitrogen gas. The dried extract was re-constituted immediately in

50 µL of water:acetonitrile:formic acid, 63:37:0.02 (vol/vol/vol), for mass spectrometric analysis. Eicosanoid analyses were conducted on a Shimadzu 40 × 3B-UPLC coupled to Sciex QTRAP 6500 Plus (Sciex, USA). Eicosanoids were separated on a Phenomenex Kinetex-C18 column (i.d. 100 × 2.1 mm, 1.7 µm) with mobile phases comprising (i) water:acetonitrile:formic acid, 63:37:0.02 (vol/vol/vol), and (ii) acetonitrile:isopropanol, 1:1 (vol/vol), as described previously (49).

Statistical analysis

The data were analyzed using GraphPad Prism 8.4.3 software. The survival of mice was analyzed via Kaplan-Meier analysis. Comparisons of survival rates between groups were analyzed using the log rank test. Comparisons between groups were analyzed using an unpaired Student's *t*-test (two-tailed). A *P*-value of <0.05 was considered to be indicative of a statistically significant result.

ACKNOWLEDGMENTS

This work was supported by the National Natural Science Foundation of China (32071152), Natural Science Foundation of Guangdong Province (2019A1515011020, 2020A1515010769, 2021A1515011424, 2021A1515010456), Foundation for Basic and Applied Basic Research of Guangzhou (202201010472), Youth Innovation Promotion Association of Chinese Academy of Sciences (2022361), and Independent Project of State Key Laboratory of Respiratory Diseases (SKLRD-Z-202225).

L.Q., L.C. and P.L. conceived the idea, designed the experiments, and interpreted the data. H.B., S.Z., Z-J.L., Y.L., Z-X.L., X.L., and Z.W. performed the experiments and collected the data. H.B., L.F., P.L., L.C., and L.Q. prepared and revised the manuscript.

AUTHOR AFFILIATIONS

[1]State Key Laboratory of Respiratory Disease, Guangzhou Institutes of Biomedicine and Health, Chinese Academy of Sciences, Guangzhou, China
[2]University of Chinese Academy of Sciences, Beijing, China

AUTHOR ORCIDs

Hemeng Bu http://orcid.org/0009-0008-2649-8069
Liqiang Feng http://orcid.org/0000-0001-6811-2074
Ling Chen http://orcid.org/0000-0003-1485-1626
Linbing Qu http://orcid.org/0000-0002-3964-1740

FUNDING

Funder	Grant(s)	Author(s)
MOST | National Natural Science Foundation of China (NSFC)	32071152	Linbing Qu
Youth Innovation Promotion Association of the Chinese Academy of Sciences (CAS YIPA)	2022361	Pingchao Li
GDSTC | Natural Science Foundation of Guangdong Province (廣東省自然科學基金)	2021A1515010456	Pingchao Li
GZST | Natural Science Foundation of Guangzhou Municipality (Guangzhou Natural Science Foundation)	202201010472	Shengnan Zhang

DATA AVAILABILITY

The lipidomic data presented in this article have been submitted to the National Genomics Data Center (https://bigd.big.ac.cn/bioproject/) under accession number

PRJCA023536. All scripts used in this study are publicly available at https://github.com/ChenLinglab/.

ETHICS APPROVAL

Animal studies were conducted in accordance with the Public Health Service Policy on Humane Care and Use of Laboratory Animals and approved by the Animal Research Committee of the Guangzhou Institute of Biomedicine and Health (IACUC no. 2021057).

ADDITIONAL FILES

The following material is available online.

Supplemental Material

Supplemental figures (JVI00198-24-s0001.docx). Figures S1 to S6.
Table S1 (JVI00198-24-s0002.docx). Primers used in this study.

REFERENCES

1. Javanian M, Barary M, Ghebrehewet S, Koppolu V, Vasigala V, Ebrahimpour S. 2021. A brief review of influenza virus infection. J Med Virol 93:4638–4646. https://doi.org/10.1002/jmv.26990
2. Belongia EA, Simpson MD, King JP, Sundaram ME, Kelley NS, Osterholm MT, McLean HQ. 2016. Variable influenza vaccine effectiveness by subtype: a systematic review and meta-analysis of test-negative design studies. Lancet Infect Dis 16:942–951. https://doi.org/10.1016/S1473-3099(16)00129-8
3. Yamayoshi S, Kawaoka Y. 2019. Current and future influenza vaccines. Nat Med 25:212–220. https://doi.org/10.1038/s41591-018-0340-z
4. Palese P. 2004. Influenza: old and new threats. Nat Med 10:S82–S87. https://doi.org/10.1038/nm1141
5. Jansen JM, Gerlach T, Elbahesh H, Rimmelzwaan GF, Saletti G. 2019. Influenza virus-specific CD4+ and CD8+ T cell-mediated immunity induced by infection and vaccination. J Clin Virol 119:44–52. https://doi.org/10.1016/j.jcv.2019.08.009
6. Alam S, Sant AJ. 2011. Infection with seasonal influenza virus elicits CD4 T cells specific for genetically conserved epitopes that can be rapidly mobilized for protective immunity to pandemic H1N1 influenza virus. J Virol 85:13310–13321. https://doi.org/10.1128/JVI.05728-11
7. Lightman S, Cobbold S, Waldmann H, Askonas BA. 1987. Do L3T4+ T cells act as effector cells in protection against influenza virus infection. Immunology 62:139–144.
8. Scherle PA, Palladino G, Gerhard W. 1992. Mice can recover from pulmonary influenza virus infection in the absence of class I-restricted cytotoxic T cells. J Immunol 148:212–217. https://doi.org/10.4049/jimmunol.148.1.212
9. Liang S, Mozdzanowska K, Palladino G, Gerhard W. 1994. Heterosubtypic immunity to influenza type A virus in mice. Effector mechanisms and their longevity. J Immunol 152:1653–1661. https://doi.org/10.4049/jimmunol.152.4.1653
10. Pizzolla A, Nguyen THO, Smith JM, Brooks AG, Kedzieska K, Heath WR, Reading PC, Wakim LM. 2017. Resident memory CD8$^+$ T cells in the upper respiratory tract prevent pulmonary influenza virus infection. Sci Immunol 2:eaam6970. https://doi.org/10.1126/sciimmunol.aam6970
11. Coulombe F, Jaworska J, Verway M, Tzelepis F, Massoud A, Gillard J, Wong G, Kobinger G, Xing Z, Couture C, Joubert P, Fritz JH, Powell WS, Divangahi M. 2014. Targeted prostaglandin E2 inhibition enhances antiviral immunity through induction of type I interferon and apoptosis in macrophages. Immunity 40:554–568. https://doi.org/10.1016/j.immuni.2014.02.013
12. Schwerbrock NMJ, Karlsson EA, Shi Q, Sheridan PA, Beck MA. 2009. Fish oil-fed mice have impaired resistance to influenza infection. J Nutr 139:1588–1594. https://doi.org/10.3945/jn.109.108027
13. Taketomi Y, Murakami M. 2022. Regulatory roles of phospholipase A_2 enzymes and bioactive lipids in mast cell biology. Front Immunol 13:923265. https://doi.org/10.3389/fimmu.2022.923265
14. Murakami M, Sato H, Taketomi Y. 2023. Modulation of immunity by the secreted phospholipase A_2 family. Immunol Rev 317:42–70. https://doi.org/10.1111/imr.13205
15. Zhao J, Zhao J, Legge K, Perlman S. 2011. Age-related increases in PGD_2 expression impair respiratory DC migration, resulting in diminished T cell responses upon respiratory virus infection in mice. J Clin Invest 121:4921–4930. https://doi.org/10.1172/JCI59777
16. Wong L-YR, Zheng J, Wilhelmsen K, Li K, Ortiz ME, Schnicker NJ, Thurman A, Pezzulo AA, Szachowicz PJ, Li P, Pan R, Klumpp K, Aswad F, Rebo J, Narumiya S, Murakami M, Zuniga S, Sola I, Enjuanes L, Meyerholz DK, Fortney K, McCray PB Jr, Perlman S. 2022. Eicosanoid signalling blockade protects middle-aged mice from severe COVID-19. Nature 605:146–151. https://doi.org/10.1038/s41586-022-04630-3
17. Snider JM, You JK, Wang X, Snider AJ, Hallmark B, Zec MM, Seeds MC, Sergeant S, Johnstone L, Wang Q, Sprissler R, Carr TF, Lutrick K, Parthasarathy S, Bime C, Zhang HH, Luberto C, Kew RR, Hannun YA, Guerra S, McCall CE, Yao G, Del Poeta M, Chilton FH. 2021. Group IIA secreted phospholipase A_2 is associated with the pathobiology leading to COVID-19 mortality. J Clin Invest 131:e149236. https://doi.org/10.1172/JCI149236
18. Suzuki N, Ishizaki J, Yokota Y, Higashino K, Ono T, Ikeda M, Fujii N, Kawamoto K, Hanasaki K. 2000. Structures, enzymatic properties, and expression of novel human and mouse secretory phospholipase A_2s. J Biol Chem 275:5785–5793. https://doi.org/10.1074/jbc.275.8.5785
19. Murakami M, Yoshihara K, Shimbara S, Lambeau G, Singer A, Gelb MH, Sawada M, Inagaki N, Nagai H, Kudo I. 2002. Arachidonate release and eicosanoid generation by group IIE phospholipase A_2. Biochem Biophys Res Commun 292:689–696. https://doi.org/10.1006/bbrc.2002.6716
20. Sato H, Taketomi Y, Ushida A, Isogai Y, Kojima T, Hirabayashi T, Miki Y, Yamamoto K, Nishito Y, Kobayashi T, Ikeda K, Taguchi R, Hara S, Ida S, Miyamoto Y, Watanabe M, Baba H, Miyata K, Oike Y, Gelb MH, Murakami M. 2014. The adipocyte-inducible secreted phospholipases PLA2G5 and PLA2G2E play distinct roles in obesity. Cell Metabolism 20:119–132. https://doi.org/10.1016/j.cmet.2014.05.002
21. Chen B, Chen Y, Rai KR, Wang X, Liu S, Li Y, Xiao M, Ma Y, Wang G, Guo G, Huang S, Chen JL. 2021. Deficiency of eIF4B increases mouse mortality and impairs antiviral immunity. Front Immunol 12:723885. https://doi.org/10.3389/fimmu.2021.723885
22. Verma V, Dileepan M, Huang Q, Phan T, Hu WS, Ly H, Liang Y. 2022. Influenza A virus activates cellular tropomyosin receptor kinase A (TrkA) signaling to promote viral replication and lung inflammation. PLoS Pathog 18:e1010874. https://doi.org/10.1371/journal.ppat.1010874
23. Wang T, Zhang J, Wang Y, Li Y, Wang L, Yu Y, Yao Y. 2023. Influenza-trained mucosal-resident alveolar macrophages confer long-term antitumor immunity in the lungs. Nat Immunol 24:423–438. https://doi.org/10.1038/s41590-023-01428-x

24. Zhi H, Qu L, Wu F, Chen L, Tao J. 2015. Group IIE secretory phospholipase A_2 regulates lipolysis in adipocytes. Obesity (Silver Spring) 23:760–768. https://doi.org/10.1002/oby.21015
25. Chen X, Liu S, Goraya MU, Maarouf M, Huang S, Chen JL. 2018. Host immune response to influenza A virus infection. Front Immunol 9:320. https://doi.org/10.3389/fimmu.2018.00320
26. Guthmiller JJ, Utset HA, Wilson PC. 2021. B cell responses against influenza viruses: short-lived humoral immunity against a life-long threat. Viruses 13:965. https://doi.org/10.3390/v13060965
27. Cox MA, Harrington LE, Zajac AJ. 2011. Cytokines and the inception of CD8 T cell responses. Trends Immunol 32:180–186. https://doi.org/10.1016/j.it.2011.01.004
28. Halle S, Halle O, Förster R. 2017. Mechanisms and dynamics of T cell-mediated cytotoxicity *in vivo*. Trends Immunol 38:432–443. https://doi.org/10.1016/j.it.2017.04.002
29. Tam VC, Quehenberger O, Oshansky CM, Suen R, Armando AM, Treuting PM, Thomas PG, Dennis EA, Aderem A. 2013. Lipidomic profiling of influenza infection identifies mediators that induce and resolve inflammation. Cell 154:213–227. https://doi.org/10.1016/j.cell.2013.05.052
30. Belkaid Y, Harrison OJ. 2017. Homeostatic immunity and the microbiota. Immunity 46:562–576. https://doi.org/10.1016/j.immuni.2017.04.008
31. Miki Y, Taketomi Y, Kidoguchi Y, Yamamoto K, Muramatsu K, Nishito Y, Park J, Hosomi K, Mizuguchi K, Kunisawa J, Soga T, Boilard E, B Gowda SG, Ikeda K, Arita M, Murakami M. 2022. Group IIA secreted phospholipase A_2 controls skin carcinogenesis and psoriasis by shaping the gut microbiota. JCI Insight 7:e152611. https://doi.org/10.1172/jci.insight.152611
32. Doré E, Joly-Beauparlant C, Morozumi S, Mathieu A, Lévesque T, Allaeys I, Duchez A-C, Cloutier N, Leclercq M, Bodein A, Payré C, Martin C, Petit-Paitel A, Gelb MH, Rangachari M, Murakami M, Davidovic L, Flamand N, Arita M, Lambeau G, Droit A, Boilard E. 2022. The interaction of secreted phospholipase A_2-IIA with the microbiota alters its lipidome and promotes inflammation. JCI Insight 7:e152638. https://doi.org/10.1172/jci.insight.152638
33. Eerola LI, Surrel F, Nevalainen TJ, Gelb MH, Lambeau G, Laine VJO. 2006. Analysis of expression of secreted phospholipases A_2 in mouse tissues at protein and mRNA levels. Biochim Biophys Acta 1761:745–756. https://doi.org/10.1016/j.bbalip.2006.04.002
34. Vijay R, Hua X, Meyerholz DK, Miki Y, Yamamoto K, Gelb M, Murakami M, Perlman S. 2015. Critical role of phospholipase A_2 group IID in age-related susceptibility to severe acute respiratory syndrome-CoV infection. J Exp Med 212:1851–1868. https://doi.org/10.1084/jem.20150632
35. Kelvin AA, Degousee N, Banner D, Stefanski E, León AJ, Angoulvant D, Paquette SG, Huang SSH, Danesh A, Robbins CS, Noyan H, Husain M, Lambeau G, Gelb M, Kelvin DJ, Rubin BB. 2014. Lack of group X secreted phospholipase A_2 increases survival following pandemic H1N1 influenza infection. Virology 454–455:78–92. https://doi.org/10.1016/j.virol.2014.01.030
36. von Allmen CE, Schmitz N, Bauer M, Hinton HJ, Kurrer MO, Buser RB, Gwerder M, Muntwiler S, Sparwasser T, Beerli RR, Bachmann MF. 2009. Secretory phospholipase A2-IID is an effector molecule of $CD4^+CD25^+$ regulatory T cells. Proc Natl Acad Sci U S A 106:11673–11678. https://doi.org/10.1073/pnas.0812569106
37. Chen L, Wu M, Zhang S, Tan W, Guan M, Feng L, Chen C, Tao J, Chen L, Qu L. 2019. Estrogen-related receptor γ regulates hepatic triglyceride metabolism through phospholipase A_2 G12B. FASEB J 33:7942–7952. https://doi.org/10.1096/fj.201802704R
38. Guan M, Qu L, Tan W, Chen L, Wong CW. 2011. Hepatocyte nuclear factor-4 alpha regulates liver triglyceride metabolism in part through secreted phospholipase A_2 GXIIB. Hepatology 53:458–466. https://doi.org/10.1002/hep.24066
39. Maseda D, Ricciotti E, Crofford LJ. 2019. Prostaglandin regulation of T cell biology. Pharmacol Res 149:104456. https://doi.org/10.1016/j.phrs.2019.104456
40. Henricks PA, Engels F, van der Vliet H, Nijkamp FP. 1991. 9- and 13-hydroxy-linoleic acid possess chemotactic activity for bovine and human polymorphonuclear leukocytes. Prostaglandins 41:21–27. https://doi.org/10.1016/0090-6980(91)90101-k
41. Chen M, Aoki-Utsubo C, Kameoka M, Deng L, Terada Y, Kamitani W, Sato K, Koyanagi Y, Hijikata M, Shindo K, Noda T, Kohara M, Hotta H. 2017. Broad-spectrum antiviral agents: secreted phospholipase A_2 targets viral envelope lipid bilayers derived from the endoplasmic reticulum membrane. Sci Rep 7:15931. https://doi.org/10.1038/s41598-017-16130-w
42. Muller VD, Soares RO, dos Santos NN, Trabuco AC, Cintra AC, Figueiredo LT, Caliri A, Sampaio SV, Aquino VH. 2014. Phospholipase A_2 isolated from the venom of *Crotalus durissus terrificus* inactivates dengue virus and other enveloped viruses by disrupting the viral envelope. PLoS One 9:e112351. https://doi.org/10.1371/journal.pone.0112351
43. Muller VDM, Russo RR, Cintra ACO, Sartim MA, Alves-Paiva RDM, Figueiredo LTM, Sampaio SV, Aquino VH. 2012. Crotoxin and phospholipases A_2 from *Crotalus durissus terrificus* showed antiviral activity against dengue and yellow fever viruses. Toxicon 59:507–515. https://doi.org/10.1016/j.toxicon.2011.05.021
44. Kim J-O, Chakrabarti BK, Guha-Niyogi A, Louder MK, Mascola JR, Ganesh L, Nabel GJ. 2007. Lysis of human immunodeficiency virus type 1 by a specific secreted human phospholipase A_2. J Virol 81:1444–1450. https://doi.org/10.1128/JVI.01790-06
45. Fenard D, Lambeau G, Valentin E, Lefebvre JC, Lazdunski M, Doglio A. 1999. Secreted phospholipases A_2, a new class of HIV inhibitors that block virus entry into host cells. J Clin Invest 104:611–618. https://doi.org/10.1172/JCI6915
46. Li X, Jiang H, Qu L, Yao W, Cai H, Chen L, Peng T. 2014. Hepatocyte nuclear factor 4α and downstream secreted phospholipase A_2 GXIIB regulate production of infectious hepatitis C virus. J Virol 88:612–627. https://doi.org/10.1128/JVI.02068-13
47. Yu L, Liu X, Ye X, Su W, Zhang X, Deng W, Luo J, Xiang M, Guo W, Zhang S, Xu W, Yan Q, Wang Q, Cui Y, Wu C, Guo W, Niu X, Zhang F, Lei C, Qu L, Chen L, Feng L. 2021. Monoclonal antibodies against Zika virus NS1 protein confer protection via Fcγ receptor-dependent and -independent pathways. mBio 12:e03179-20. https://doi.org/10.1128/mBio.03179-20
48. Kim MV, Ouyang W, Liao W, Zhang MQ, Li MO. 2014. Murine *in vivo* $CD8_+$ T cell killing assay. Bio Protoc 4:e1172. https://doi.org/10.21769/BioProtoc.1172
49. Lam SM, Wang Z, Li J, Huang X, Shui G. 2017. Sequestration of polyunsaturated fatty acids in membrane phospholipids of *Caenorhabditis elegans* dauer larva attenuates eicosanoid biosynthesis for prolonged survival. Redox Biol 12:967–977. https://doi.org/10.1016/j.redox.2017.05.002
50. Yue H, Jansen SA, Strauss KI, Borenstein MR, Barbe MF, Rossi LJ, Murphy E. 2007. A liquid chromatography/mass spectrometric method for simultaneous analysis of arachidonic acid and its endogenous eicosanoid metabolites prostaglandins, dihydroxyeicosatrienoic acids, hydroxyeicosatetraenoic acids, and epoxyeicosatrienoic acids in rat brain tissue. J Pharm Biomed Anal 43:1122–1134. https://doi.org/10.1016/j.jpba.2006.10.009